08,10

Magnetic and magnetoresistive properties of multilayer nanostructures $(Co/CoO)_{60}$

© Y.E. Kalinin[1], K.S. Gabriels[1], V.A. Makagonov[1,¶], V.A. Foshin[1], R.B. Morgunov[2], M.V. Bakhmetiev[2], E.V. Dvoretskaya[2], I.I. Khodos[2]

[1] Voronezh State Technical University, Voronezh, Russia
[2] Federal Research Center of Problems of Chemical Physics and Medicinal Chemistry RAS, Chernogolovka, Russia

¶ E-mail: vlad_makagonov@mail.ru

Received January 11, 2025
Revised April 18, 2025
Accepted April 24, 2025

The structure and electrical, magnetic, and magnetoresistive properties of thin films $(Co/CoO)_{60}$ were studied. Using X-ray diffraction and transmission electron microscopy methods, it was shown that the obtained films are multilayered, and an increase in the thickness of the Co interlayer to 0.8 nm leads to a transition from island layers of Co in a continuous CoO matrix to a multilayer structure. The study of electrical properties showed that there is a consistent change of the dominant transfer mechanism in the studied system from the hopping mechanism of conductivity along localized states near the Fermi level with a variable hop length to hops along the nearest neighbors. The study of magnetic and magneto-optical properties showed the presence of magnetic anisotropy in the samples near the percolation threshold and beyond it. The magnetoresistance is determined by the mechanism of spin-dependent tunneling between granules and clusters of metallic Co for samples up to the percolation threshold, and beyond the threshold it is determined by the anisotropic magnetoresistance of percolation networks of ferromagnetic Co and the Lorentz magnetoresistance.

Keywords: multilayer nanostructures, specific electrical resistance, percolation threshold, magnetic properties, anisotropic magnetoresistance.

DOI: 10.61011/PSS.2025.04.61274.9-25

1. Introduction

Composite nanostructured ferromagnetic-dielectric materials have attracted the interest of many researchers in recent years [1–3]. The transport and magnetic properties are of interest, which are key to modern solid-state electronics, in the development of which spin-dependent processes occurring at interfaces in heterostructures are becoming increasingly important [4,5]. Knowledge of the magnetic and electrical properties of thin composite films is also necessary to understand and explain the mechanisms of reflection and absorption of electromagnetic waves [6,7].

The special attraction of nanostructured ferromagnetic-dielectric composites lies in the possibility of creating materials with unique and preset properties, which, combined with their high resistance to corrosion and oxidation, can open up new horizons for their application in various fields such as electronics, energy, sensors, strain electronics and catalytic processes. Experimental studies of composite films and the search for a relationship between constitutive parameters (thickness of films, layers, and interlayers) and magnetic and electrical properties will make it possible to optimize the processes of industrial synthesis of such structures for specific practical applications in the future [8–13]. To obtain a complete picture of the physical properties and processes accompanying the synthesis of such composites, it is important to study the parameters of their formation and the mechanisms of the influence of morphology on electrical and magnetic properties.

Multilayer structures made of cobalt layers with layers of antiferomagnetic cobalt oxide are of particular scientific interest, since the effect of magnetic proximity is possible in ferromagnetic/antiferromagnetic structures. The effect of magnetic proximity occurs between two heterogeneous magnetic components at the atomic level and due to the appearance of exchange interactions between them [14,15]. It can manifest itself simultaneously with the exchange bias effect, sometimes called unidirectional or exchange anisotropy.

This work is devoted to the synthesis and study of the electrical and magnetoresistive properties of multilayer structures of ferromagnetic cobalt with layers of antiferomagnetic cobalt oxide.

2. Samples and experimental method

Thin films $(Co/CoO)_{60}$ were obtained by ion beam sputtering of a ceramic target of CoO and metallic Co in an argon atmosphere with a purity of 99.998 % at

a pressure of $P = 64$ MPa onto an additionally unheated substrate [16]. The temperature of the substrate during the sputtering process did not exceed 400 K. The targets were fixed on water-cooled copper bases with a size of $280 \times 80\,mm^2$ and placed in different spray positions in a vacuum chamber. The substrate was moved from one spray position to another by rotating the substrate holder around the axis of the spray chamber for a layer-by-layer deposition. Deposition was carried out on single-crystal silicon substrates with a crystallographic orientation of (100) to study the structure and a crystal to study the electrophysical properties. A Λ-shaped screen was installed between the Co target and the substrate holder to obtain different thicknesses of Co layers during a single sputtering process. The rotation speed was 0.1 rev/min. The number of revolutions of the substrate holder determined the number of bilayers in the multilayer film and was 60, which is reflected by the subscript in the designation of the studied heterostructures $(Co/CoO)_{60}$.

For a preliminary assessment of the thickness of the layers, individual Co and CoO films were pre-sputtered with the process parameters previously selected for the multilayer structure. The thickness of the obtained films was measured using an optical interferometer MII−4 on samples located on a substrate holder along a straight, parallel axis Λ-shaped screen. The thickness measurement points were fixed relative to the location of the substrate and the target. The measured film thickness data was approximated. Knowing the number of revolutions of the substrate holder, the thickness of the film obtained during a single passage of the substrate of the material application zone, i. e. the thickness of the monolayer of one of the sprayed components, was calculated. The thickness of the monolayer of the second component of the multilayer structure was determined in a similar way. The value of the monolayer thickness of Co varied from 0.2 to 1.4 nm for the obtained thin films, and CoO was ≈ 2.4 nm. It should be noted that the monolayer thickness value obtained in this way is equivalent and does not take into account the possibility of island growth, i. e. it is the thickness of a thin film applied in one revolution of the substrate holder, provided that this film is continuous. Thus, given that the thickness of the CoO interlayers is greater than the thickness of the Co interlayers, it is likely that with an increase in the thickness of the Co interlayer, a transition occurs from a two-phase film of island layers of Co in a continuous matrix of CoO formed during layer-by-layer deposition to a multilayer structure consisting of continuous layers of metallic Co and non-conductive electric current CoO. Therefore, in the future it will be advisable to consider the experimental results obtained depending on the equivalent thickness of the Co interlayer, as the parameter that most critically affects the structure and physical properties of the thin films under study.

The local chemical composition was determined using a JEOLSuperprobe-733 scanning electron probe microanalyzer. The structure of the resulting thin films was studied using X-ray diffraction (XRD) and electron microscopic analysis (TEM). To study the structure of composites by the XRD method, thin films deposited on a single-crystal silicon substrate with a crystallographic orientation of (100) were used.

The electrical resistivity was measured using a four-wire DC circuit using a universal digital multimeter B7−78/1 along the plane of the film and the layers of the multilayer structure. Thermal EMF from the thickness of the films was measured using a differential method (silver wire with a purity of 99.99 % was used as the material of the cold and hot probes). The relative measurement error did not exceed 3 %.

The images of local magnetization were obtained using a NEOARK Neomagnesia Lite BH-753 microscope with the possibility of studying the meridional magneto-optical Kerr effect (MOKE). Magnetic hysteresis loops in the temperature range 2−300 K were obtained using a Cryogen Free Measurement System vibration magnetometer (Cryogenic Ltd., Great Britain).

3. Experimental results and their discussion

3.1. Structure of thin films $(Co/CoO)_{60}$

Figure 1 shows X-ray diffraction patterns from thin films $(Co/CoO)_{60}$. The figures for the curves show the values of the equivalent thickness of the Co interlayers (h_{Co}). The analysis of small-angle diffraction patterns shows that a layered structure is observed in thin films $(Co/CoO)_{60}$, as evidenced by the presence of maxima in the range of Bregg angles of 1−7° and an increase in their intensity with the increase of thickness of the Co interlayer. The period of multilayer structures $(Co/CoO)_{60}$ (bilayer thickness), calculated from Figure 1, *a*, varied from 2.6 to 3.8 nm. The total number of bilayers from the production conditions was 60, which corresponds to the thickness range of all films from 156 to 228 nm. The shape of the peaks is complex, which in general can be interpreted as some deviation from the periodicity (irregularity of the thicknesses of individual layers associated with their island growth). Probably, the asymmetry of the maxima is also a consequence of the formation of additional layers at the interfacial boundaries of Co−CoO, similar in composition to Co_3O_4. The results of the analysis of X-ray diffraction patterns in the region of average Bregg angles of 30−80° do not contradict our assumptions.

Indeed, for all the studied samples, pronounced peaks of cubic CoO (111) and CoO (222) are observed in the area of angles 30−80°, indicating a strong uniaxial texture with the axis ⟨111⟩.

In addition to the cubic CoO phase, maxima were identified on the diffraction patterns of the studied samples with Co interlayer thicknesses of more than 0.8 nm Co_3O_4.

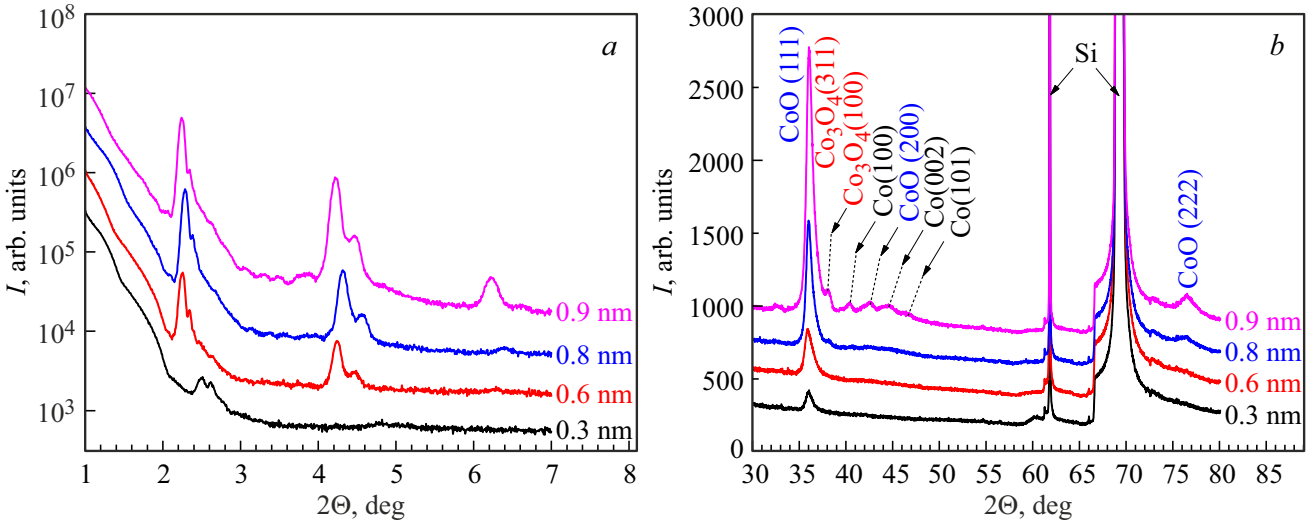

Figure 1. X-ray diffraction patterns from thin films $(Co/CoO)_{60}$, measured in the region of small (a) and medium (b) Bragg angles. The figures for the curves show the values of the equivalent thickness of the Co layers.

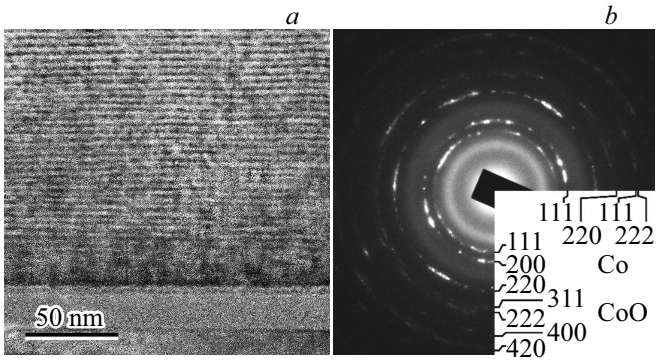

Figure 2. Light-field TEM cross-sectional image (a) and electron diffraction pattern (b) from a multilayer structure $(Co/CoO)_{60}$ ($h_{Co} = 0.6$ nm).

As for the metallic phase of the studied thin films, for samples with an equivalent thickness of the Co layer not exceeding 0.8 nm (Figure 1, b) in the range of 40–50°, maxima from metallic cobalt are not observed and become distinguishable on diffractograms only with equivalent interlayer thicknesses of more than 0.8 nm. It should be noted that the angular position of the Co reflexes does not exactly match the tabular data, which may indicate the presence of macro stresses in the multilayer film itself.

Studies of the structure by transmission electron microscopy (TEM) confirmed the formation of Co interlayers and a multilayer structure (Figure 2, a), and fast electron diffraction patterns — the crystal structure of Co and Co layers (Figure 2, b).

The thicknesses of the Co and CoO interlayers obtained from TEM images for the sample under study are consistent with the results obtained from X-ray diffraction patterns in the region of small Bragg angles (Figure 1, a).

3.2. Electrical properties of thin films $(Co/CoO)_{60}$

As noted earlier, a layered structure is formed in case of thin films $(Co/CoO)_{60}$, while an increase in the equivalent thickness of the Co interlayer is accompanied by a transition from island layers of Co in a continuous CoO matrix formed during layer-by-layer deposition to a multilayer structure consisting of continuous layers of metallic Co and non-conductive electric current CoO. Such changes in the morphology of the obtained thin films should radically affect the electrical, magnetic and other physical properties of the obtained thin films. Figure 3 shows the dependences of the electrical resistivity and thermal EMF of thin films $(Co/CoO)_{60}$ on the equivalent thickness of the Co interlayer (h_{Co}). The sign of thermal EMF in synthesized thin films is negative, which indicates the dominant contribution of electrons to electrical transfer.

The obtained dependences are typical for percolation systems, for which the change in electrical resistivity during transition through the percolation threshold changes by several, in our case by almost eight orders of magnitude. In this case, the middle of the site of the sharpest change in electrical resistivity and thermal EMF can be interpreted as the percolation threshold in the metal-dielectric system associated with the transition from island Co layers to solid ones. In our case, such a transition occurs with an equivalent thickness of the Co interlayer equal to ≈ 0.8 nm, which is accompanied by a sharp decrease in the modulus of the thermal EMF value and a weak dependence on the equivalent thickness of the Co interlayer in the region of $h_{Co} > 0.8$ nm. At the same time, the thermal EMF values of the samples beyond the percolation threshold are characteristic of the thermal EMF values of pure cobalt [17].

The temperature dependences of the electrical resistivity were studied for determining the characteristics of elec-

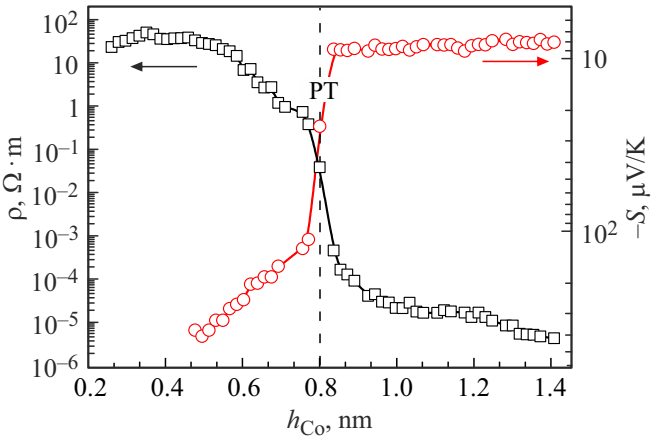

Figure 3. The dependences of the electrical resistivity ρ and thermal emf S of thin films $(Co/CoO)_{60}$ on the equivalent thickness of the Co interlayer (h_{Co}). The dashed line with the PT designation indicates the percolation threshold of the system $_{60}$.

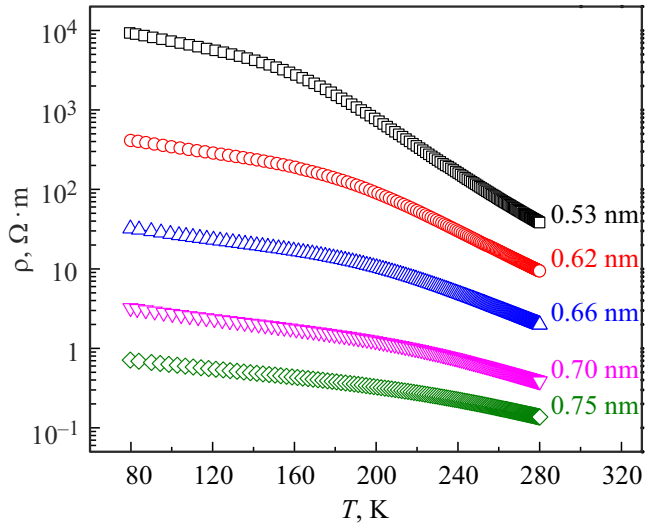

Figure 4. Temperature dependences of the electrical resistivity of thin films $(Co/CoO)_{60}$. The figures for the curves show the values of the equivalent thickness of the Co layers.

trical transfer in the obtained structures. For multilayer heterostructures $(Co/CoO)_{60}$ with an equivalent thickness of less than 0.8 nm (up to the percolation threshold), the electrical resistivity decreased with the increase of the temperature (Figure 4), and for samples with an equivalent thickness of more than 0.8 nm, the temperature coefficient was positive (not shown in the figure), as is the case in metals.

The dominant mechanisms of electrical transfer was analyzed by re-arranging the dependencies $\rho \propto f(T)$ of the samples up to the percolation threshold in coordinates $\ln\rho \propto f(T^{-n})$, where n was equal to 1/4, 1/3, 1/2, 1, and also $\ln\rho \propto f(\ln T)$.

An analysis of the data in Figure 4 showed that in the temperature range of 80–140 K, the electrical resistivity is approximated by a straight line in coordinates $\ln\rho \propto f(T^{-1/4})$ (Figure 5, *a*), which indicates a hopping the mechanism of conduction of charge carriers with variable hopping length over localized states lying in a narrow energy band near the Fermi level, and in the temperature range 140–280 K — dependence $\ln\rho \propto f(1/T)$ (Figure 5, *b*).

If fulfilment of the „1/4 law“ is interpreted as a sign of hopping conductivity on the localized states in a narrow energy band near the Fermi level (Mott conductivity), then the expression for conductivity is as follows [18]:

$$\sigma = e^2 \cdot R^2 \cdot \nu_{\text{ph}} \cdot g(E_F) \cdot \exp\left(-\frac{B}{T}\right)^{1/4}, \qquad (1)$$

where

$$B = \frac{21}{a^3 \cdot k \cdot g(E_F)}, \qquad (2)$$

where e is the electron charge, R is the hopping distance, ν_{pv} is the phonon interaction spectrum factor, T is the absolute temperature, $g(E_F)$ is the density of states at the Fermi level, a is the radius of localization of the electron wave function, k is the Boltzmann constant.

The values of the parameter B for the studied film compositions were determined from Figure 5, *a*. Let us estimate the density of localized states knowing B and assuming that the process of charge carrier transfer for samples up to the threshold is limited by hops between Co nanocrystallites in island layers in a continuous CoO matrix. The localization radius is assumed to be equal to the size of the Co crystallites, which in our case are proportional to the average equivalent thickness of the Co interlayers and equal to ≈ 0.6 nm. The evaluation results are shown in Figure 6, *a*.

We shall also estimate the average hop energy that shall be as follows for the hops with a variable hop distance:

$$W_M = \frac{1}{4} kT \left(\frac{B}{T}\right)^{1/4} \qquad (3)$$

and the average hopping length of charge carriers at a temperature of $T = 100$ K according to the formula:

$$R_M = \frac{3}{8} a \left(\frac{B}{T}\right)^{1/4}. \qquad (4)$$

The results of the assessments are shown in Figure 6. A distinctive feature of all the dependences obtained is saturation when the value of the equivalent thickness of the Co interlayers approaches the percolation threshold. Thus, the values of the density of localized states at the Fermi level tend to the values $g(E_F) \approx 10^{23}$ eV$^{-1} \cdot$ cm^{-3} characteristic of metallic cobalt [19] with an increase of the equivalent thickness of the Co interlayers.

As noted above, the temperature dependences of the electrical resistivity of the studied thin films in the temperature range 140–280 K obey the Arrhenius dependence $(\ln\rho \propto 1/T)$ (Figure 5, *b*).

If the designated temperature interval is treated as a region of hopping conductivity on the nearest neighbors,

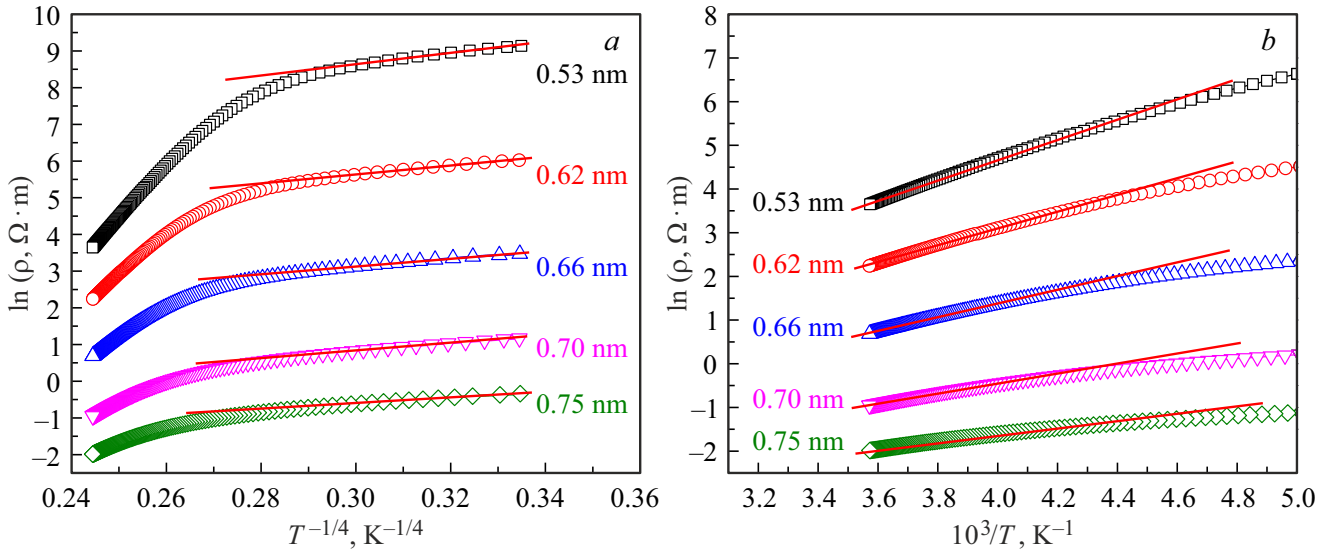

Figure 5. Temperature dependences of the electrical resistance of thin films $(Co/CoO)_{60}$, represented in coordinates $\ln\rho \propto f(T^{-1/4})$ (a) and $\ln\rho \propto f(1/T)$ (b). The figures for the curves show the values of the equivalent thickness of the Co layers.

then, according to [18], the following equation shall be true for the conductivity (5):

$$\sigma = \sigma_0 \exp\left(\frac{W_{NNH}}{k_B T}\right), \tag{5}$$

where W_{NNH} is the hop activation energy set for the hops on the nearest neighbors by the following equation:

$$W_{NNH} = \frac{3}{4\pi R_0^3 g(E_F)}, \tag{6}$$

where R_0 is the average distance between the nearest neighbors, $g(E_F)$ is the density of states at the Fermi level.

Using formulas (5) and (6), from Figure 5, b we estimate the values of the average distance between the nearest neighbors, the activation energy of the hop, the results are presented in Figure 7.

It should be noted that the estimates of the parameters of hopping electrical transport shown in Figures 6 and 7 are of an exclusively qualitative nature, since they do not take into account the morphological features of electrical transport, in particular, the layering of the structures studied, and the formulas applied are valid only for homogeneous substances. Nevertheless, from the estimates of the parameters of hopping conduction with variable hopping length shown in Figures 6 and 7, it follows that an increase in the equivalent thickness of the Co interlayers leads to an increase in the density of localized states near the Fermi level and a decrease in the energy and average hopping length. When switching to hopping along the nearest neighbors, the hop activation energy increases, and the average hopping radius decreases for all samples with an equivalent layer thickness up to the percolation threshold.

3.3. Magnetic properties of thin films $(Co/CoO)_{60}$

Figure 8, a shows the hysteresis loop of the magneto-optical Kerr effect (MOKE) of a multilayer film $(Co/CoO)_{60}$ with an equivalent thickness of the Co interlayer equal to 0.7 nm, i. e. near the percolation threshold. The inset shows a measurement scheme in case of change of the angle θ between an external magnetic field and one of the sides in the sample plane (inset in Figure 8, a). Figure 8, b shows images of domains in polarized microscope light based on the Kerr effect in magnetic fields +151.1 (*1*), −79.6 (*2*), −148.2 (*3*), −63.3 (*4*), +61.6 (*5*) and +152.2 Oe (*6*).

The dark and light regions correspond to opposite directions of magnetization lying in the plane of the film. A change in the magnetic field causes the dark field to grow and the light field to be suppressed in positive fields and the reverse process in negative fields. A change in the direction of magnetization is accompanied by the propagation of nuclei with dimensions $\approx 1-2\,\mu$m.

Figure 9 shows the MOKE hysteresis loops of the same sample with a change of θ from 0 to 90° at room temperature. The study of the magneto-optical Kerr effect showed the presence of magnetic anisotropy, with the easy axes (EA) and hard axis (HA) located in the plane of the film and perpendicular to each other (Figure 9).

Since the MOKE method allows high-speed recording of hysteresis loops on the local surface of the sample, magnetization surges were detected (Figure 9 at $\theta = 0°$, $\theta = 40°$), which amount to $\Delta M \approx 0.2\,\%$. Short duration of ≈ 2 s is the main unusual feature of the hops. This circumstance does not allow standard automation of registration and mathematical processing of magnetization surges. The magnetization surge may be caused by the competition of individual nuclei of the magnetization of insular Co, or

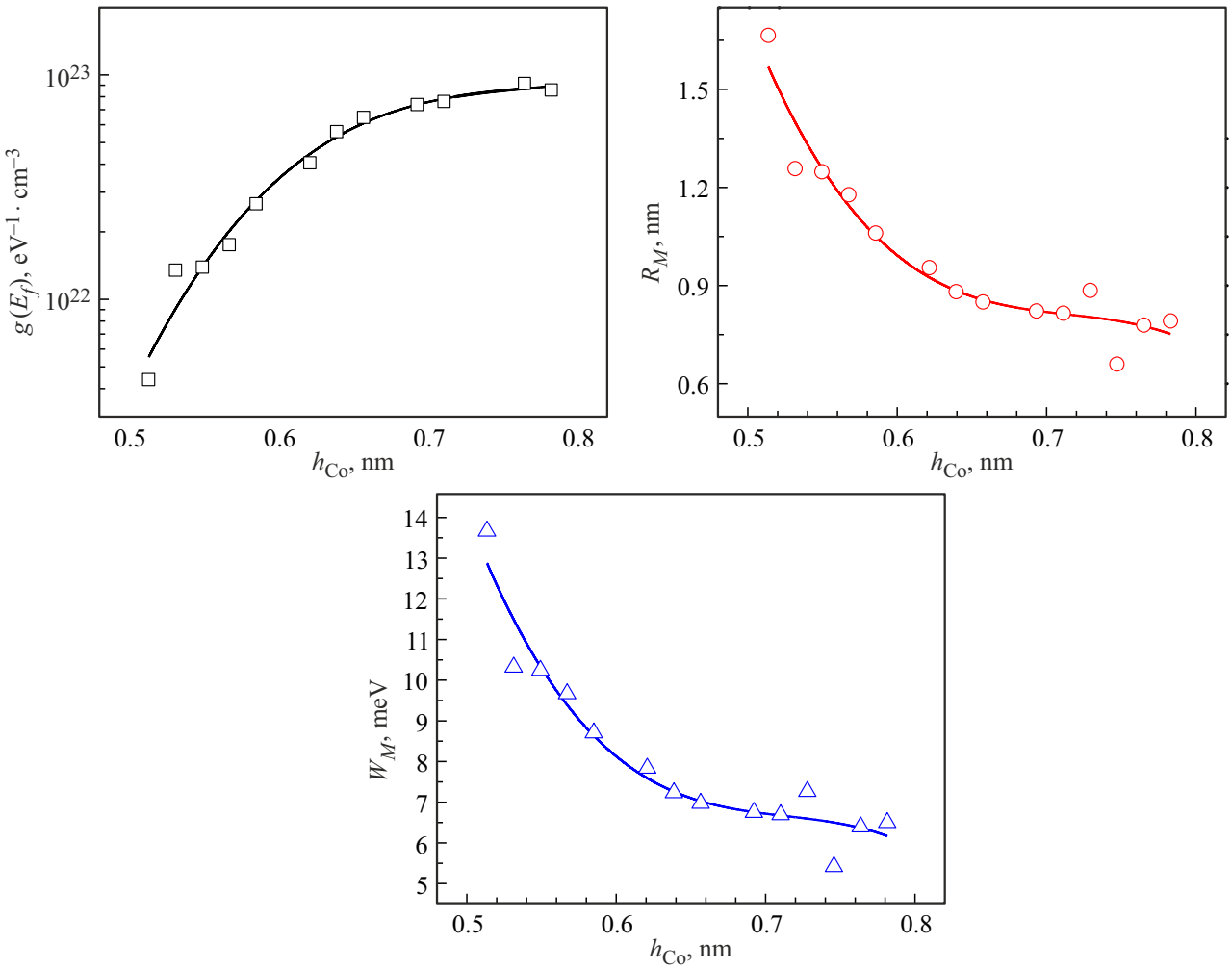

Figure 6. Parameters of thin films $(Co/CoO)_{60}$ calculated according to the hopping conduction model for localized states in a narrow energy band near the Fermi level, depending on the equivalent thickness of the Co interlayers.

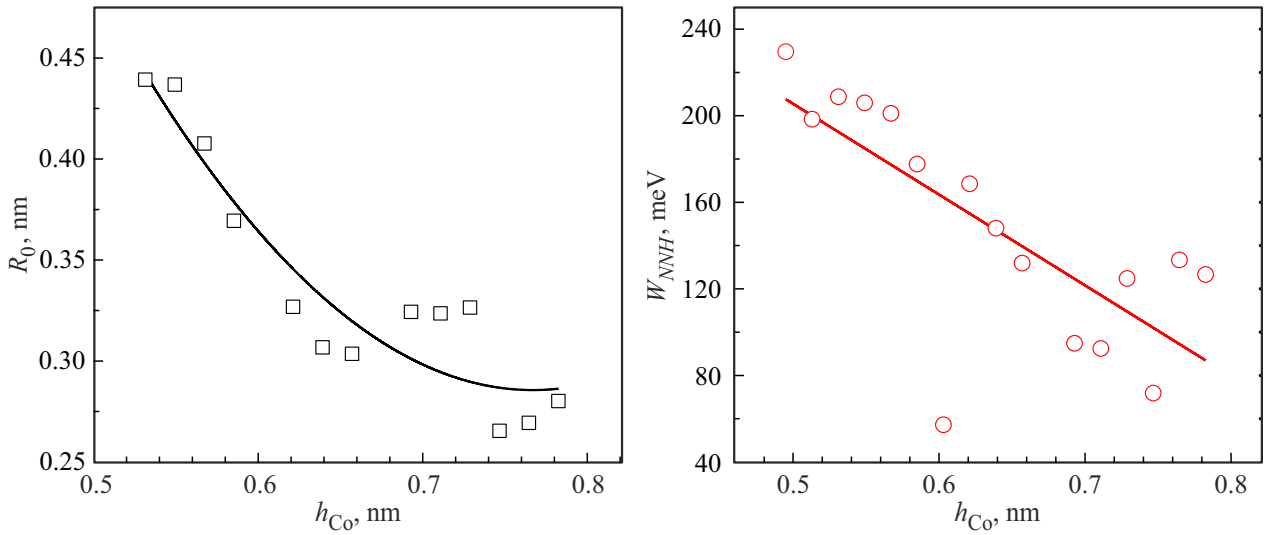

Figure 7. Parameters of thin films $(Co/CoO)_{60}$ calculated according to the nearest neighbor hopping conductivity model, depending on the equivalent thickness of the Co interlayers.

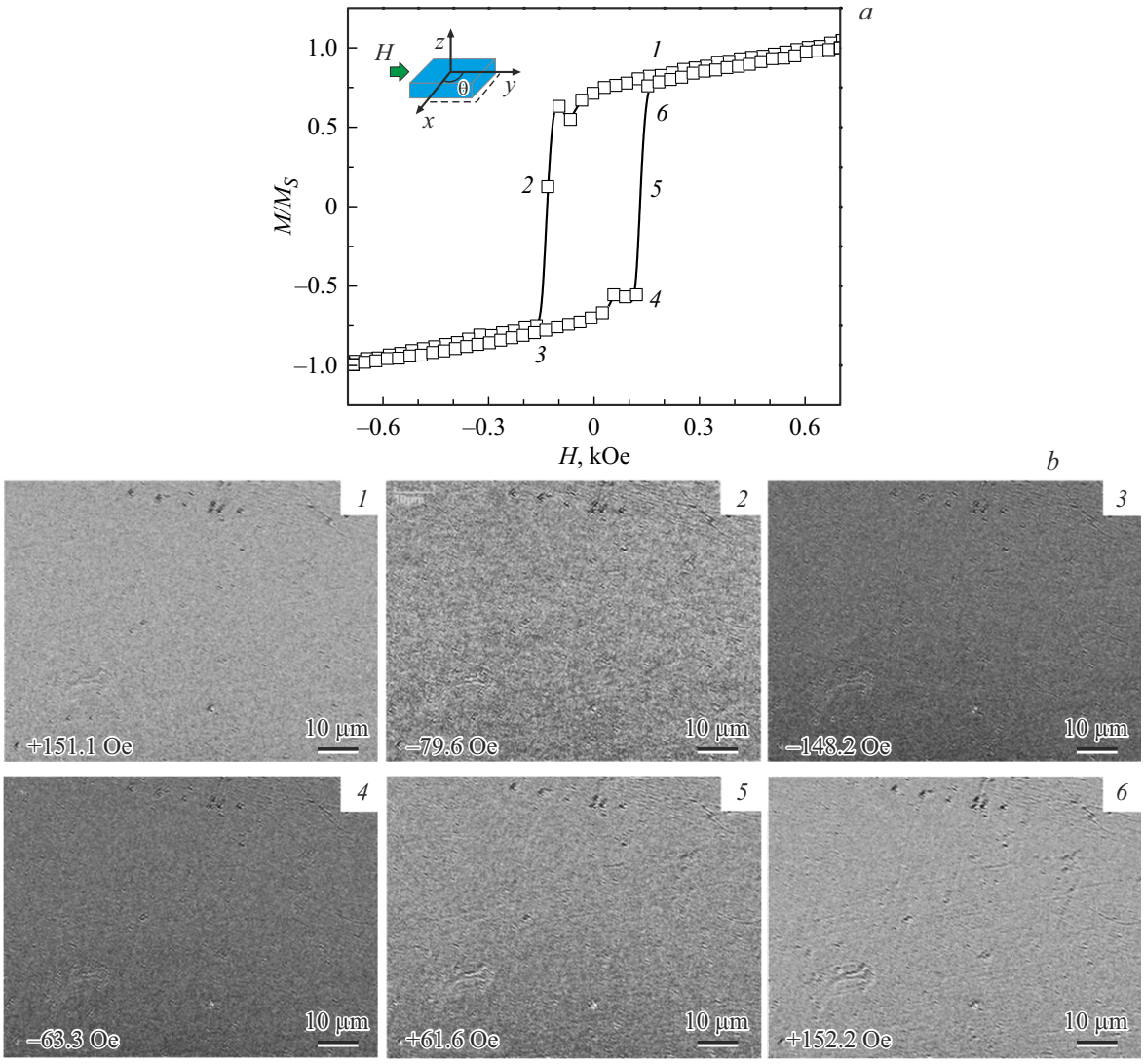

Figure 8. MOKE hysteresis loop of a multilayer film $(Co/CoO)_{60}$ with an equivalent thickness of the Co interlayer equal to 0.7 nm, i. e. near the percolation threshold (*a*) — the insert shows a measurement scheme when the angle changes θ between the external magnetic field and one of the sides in the sample plane (insert in Figure 8, *a*). Images of domains (*b*) in polarized microscope light based on the Kerr effect in magnetic fields +151.1 (*1*), −79.6 (*2*), −148.2 (*3*), −63.3 (*4*), +61.6 (*5*) and +152.2 Oe (*6*).

separate quasi-states of some insular clusters of Co in the volume of the sample.

The hysteresis loops of the CoO/Co sample up to the percolation threshold in the temperature range of 2−300 K, measured using a vibration magnetometer, showed the presence of ferromagnetism up to $T = 100$ K and its absence at higher temperatures, which is characteristic of the superparamagnetic state of the sample when a composite is formed instead of a multilayer structure Co-CoO with a cobalt oxide matrix and pure cobalt granules. It is worth noting that when recording hysteresis loops with a vibrating magnetometer, no magnetization surges were recorded, since the recording speed by this method is much lower than that of MOKE.

As examples, Figure 10 shows the magnetization curves for a sample of a multilayer film $(Co/CoO)_{60}$ up to the percolation threshold, measured using a vibration magnetometer.

An interesting fact is that for a multilayer film $(Co/CoO)_{60}$, no effects of magnetic proximity and exchange displacement were recorded before and near the percolation threshold. This was probably the case, since experimental observation of these effects implies cooling of the sample below the CoO blocking temperature in a magnetic field. In our experiments, no pre-cooling in a magnetic field was performed before recording hysteresis loops.

3.4. Magnetoresistance of thin films $(Co/CoO)_{60}$

The dependences of the electrical resistance of synthesized films on the magnitude of the external magnetic field were studied at various mutual orientations of the magnetic

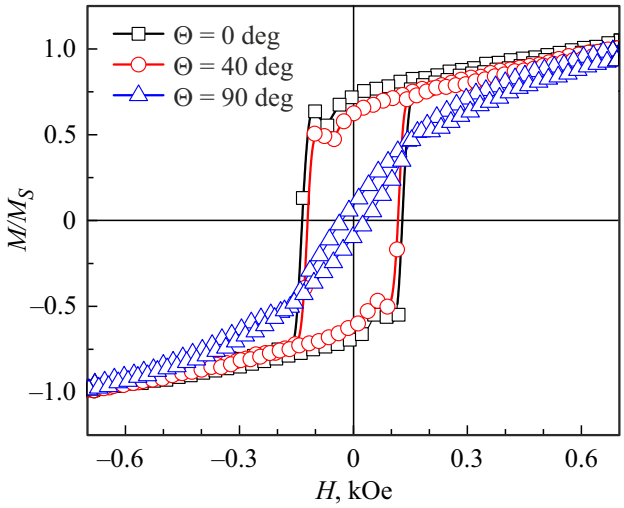

Figure 9. MOKE hysteresis loops for a sample of a multilayer film $(Co/CoO)_{60}$ with an equivalent thickness of the Co interlayer equal to 0.7 nm, i. e. near the percolation threshold when the angle changes θ between the external magnetic field and the sample plane from 0 to 90° at room temperature. The external magnetic field lies parallel to the sample plane.

field, electric current, and film plane: the magnetic field is perpendicular to the sample plane and the direction of the electric current ($H \perp$ pl, $H \perp I$) (Figure 11, *a*), the magnetic field is parallel to the sample plane and the direction of the electric current ($H \parallel$ pl, $H \parallel I$) (Figure 11, *b*), the magnetic field is parallel to the sample plane and perpendicular to the direction electric current ($H \parallel$ pl, $H \perp I$) (Figure 11, *c*).

The following expression was used to determine the magnitude of the magnetoresistance MR):

$$MR = [(R(H) - R(0))/R(0)] \cdot 100\,\%, \qquad (7)$$

where $R(H)$ and $R(0)$ are the electrical resistance values measured in a magnetic field and without a field, respectively.

An analysis of the dependences of the electrical resistance of thin films $(Co/CoO)_{60}$ on the strength of an external magnetic field at a temperature of 300 K showed that in films up to the percolation threshold (with an equivalent thickness of the Co interlayer less than ~ 0.8 nm) MR is negative and isotropic, i. e. it does not depend on the

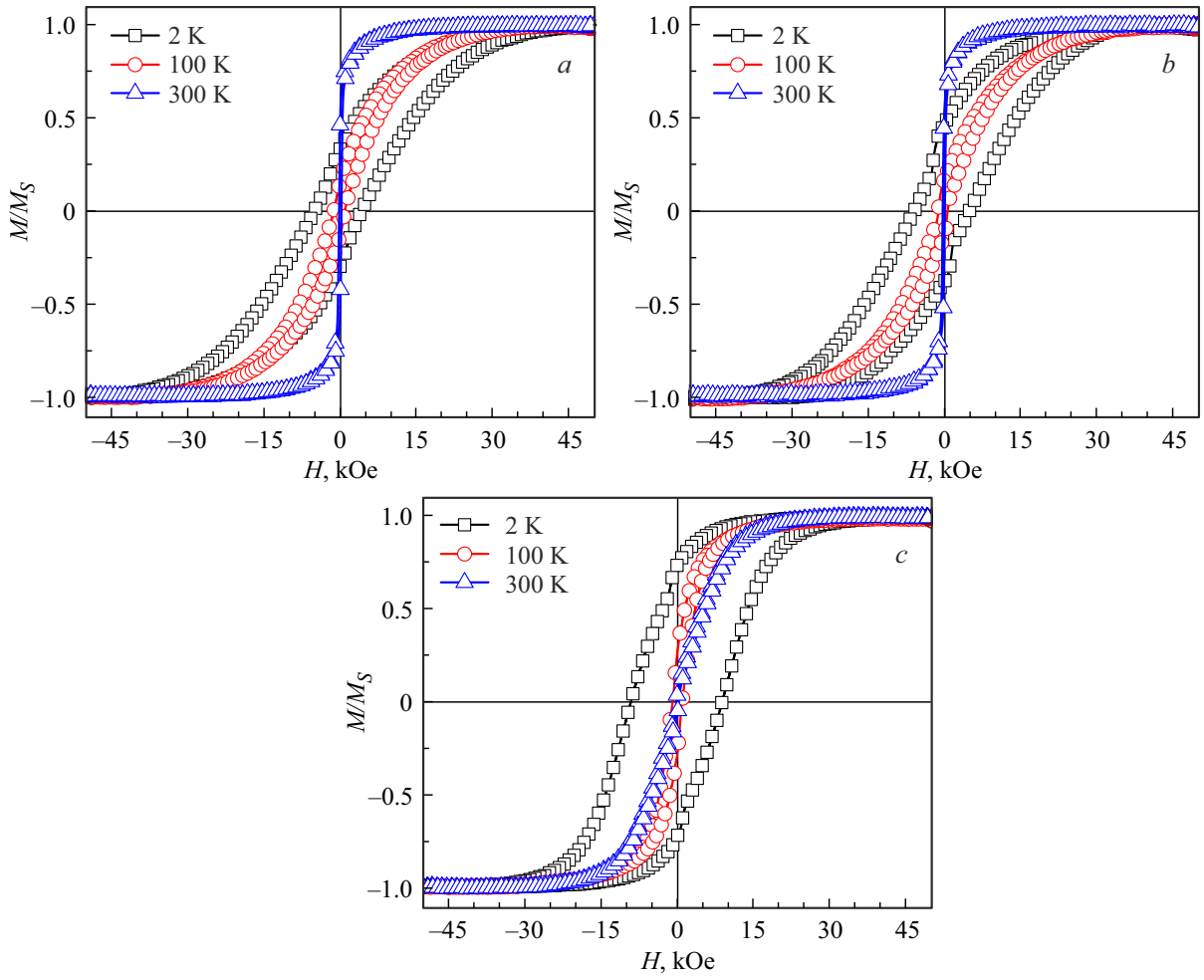

Figure 10. Hysteresis loops in the temperature range 2–300 K for a sample of a multilayer film $(Co/CoO)_{60}$ with an equivalent thickness of the Co interlayer equal to 0.7 nm, i. e. near the percolation threshold. The external magnetic field is directed parallel to the sample plane at $\theta = 0$ deg (*a*), at $\theta = 90$ deg (*b*) and perpendicular to the sample plane (*c*).

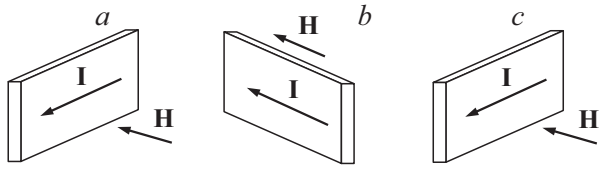

Figure 11. Schematic images explaining the methodology for studying the dependences of magnetoresistance on the strength of an external magnetic field at different orientations of the field, electric current and film plane: $(H \perp \text{pl},\ H \perp I)$ (a), $(H \parallel \text{pl},\ H \parallel I)$ (b), $(H \parallel \text{pl},\ H \perp I)$ (c).

mutual orientation of the magnetic field, current, and film plane in the field strength range up to 9 kOe (Figure 12). Lower values of the MR measured at a field strength of the order of 9 kOe when the magnetic field is oriented perpendicular to the film plane ($H \perp$ pl Figure 12, a) in comparison with the case when the magnetic field was directed along the film plane ($H \parallel$ pl Figure 11, b), due to the influence of the demagnetizing factor. The areas of positive magnetoresistance (PMR) characterized by the presence of a maximum in the field region of the order of 3,kOe, which is also isotropic appear on the field dependences of threshold films $(Co/CoO)_{60}$ with a decrease in temperature. A possible explanation for such MR dependences of subthreshold films $(Co/CoO)_{60}$ may be the presence in the structure of cobalt interlayers not only individual Co nanogranules, but also Co clusters with significantly different magnitudes of magnetic anisotropy and dipole-dipole interaction between clusters and nearby granules, as was the case in nanogranulated composites of $Co\text{-}Al_2O_n$ [20].

For samples with an equivalent Co layer thickness of more than 0.8nm, i. e. those located beyond the percolation threshold, in contrast to the pre-threshold ones, anisotropic MR was detected, while not only the magnitude but also the sign of the MR are determined by the mutual orientation of the current, magnetic field and sample plane: for the case $H \perp$ pl, $H \perp I$ MR is positive, while for $H \parallel$ pl, $H \parallel I$ — is negative. The MR value of the threshold samples did not exceed modulo $\approx 0.07\,\%$, which is more than an order of magnitude less than the MR value for samples up to the percolation threshold. Unlike thin films of $Co_n(CoO)_{100-n}$ obtained by ion beam sputtering of a composite target [4], thin films $(Co/CoO)_{60}$ have hysteresis based on $MC(H)$, measured at room temperature, were not detected. However, the MR hysteresis of the pre-percolation samples appears when measured at low temperatures (77 K), as well as the positive component (Figure 12, c, d).

The cobalt interlayers are not continuous with an equivalent thickness of $h_{Co} < 0.8$ nm. In such films, cobalt atoms assemble into granules and clusters separated from each other by a thin dielectric layer. Since the thickness of the CoO interlayers in the resulting thin films is ≈ 2.4 nm, the probability of tunneling between granules of different layers is significantly less than the probability of tunneling between granules of the same layer. The sizes of granules and clusters increase with an increase in the equivalent thickness of the cobalt layers, the distance between them decreases, which leads to the occurrence of a strong dipole-dipole interaction both between granules and clusters within the interlayers and between layers, causing the presence of ferromagnetic ordering and a decrease in the magnitude of tunneling magnetoresistance.

The electrical and magnetic properties of the obtained thin films $(Co/CoO)_{60}$ can be determined by quasi-flat layers of metallic cobalt with a further increase in the equivalent thickness of the Co interlayers at $h_{Co} > 0.8$ nm for samples beyond the percolation threshold. It should also be noted that during layer-by-layer deposition, the cluster shape will be predominantly two-dimensional, which should lead to the appearance of strong magnetic anisotropy of the obtained films and, as a result, the occurrence of anisotropic MR (AMR) [21,22].

AMR is typical for ferromagnetic materials, where the electrical resistance depends on the angle between the direction of magnetization of the sample and the external magnetic field. The reason lies in the spin-orbit interaction of electrons, which leads to spin-dependent scattering of electrons (the scattering coefficient for spins co-directional and counter-directional with respect to the magnetization of the sample will be different). Magnetic anisotropy is particularly high in ferromagnetic single crystals [23,24], where it manifests itself in the presence of axes of light magnetization, along which the vectors of spontaneous magnetization of ferromagnetic domains are directed.

Indeed, AMR was detected for samples near and beyond the percolation threshold (Figure 13, a). In the case when the magnetic field is directed along the film plane, the MR was negative regardless of the mutual orientation of the magnetic field and the electric current (dependences *1, 2* and *4, 5* Figure 13, a), however, the maximum value of MC depended on the direction of passage of the electric current relative to one of the sides of the sample, which may indicate the presence of magnetic anisotropy in the film plane. The negative MR decreased as the thickness of the Co layer increased (Figure 12).

The study of the magneto-optical Kerr effect has shown the presence of magnetic anisotropy in samples near and beyond the percolation threshold. In this case, the axes of light (easy axis) and hard (relative) magnetization are in the plane of the film and perpendicular to each other (Figure 13, b). However, as can be seen from Figure 9, EA form a cone with a sufficiently large angle of solution (more than 80 degrees). It should be clarified that the observed EA and HA are projections onto the film plane. It is not possible to determine the spatial location of the EA and HA, i. e. their angular deviation relative to the film plane, due to the influence of the sample shape factor (demagnetizing factor).

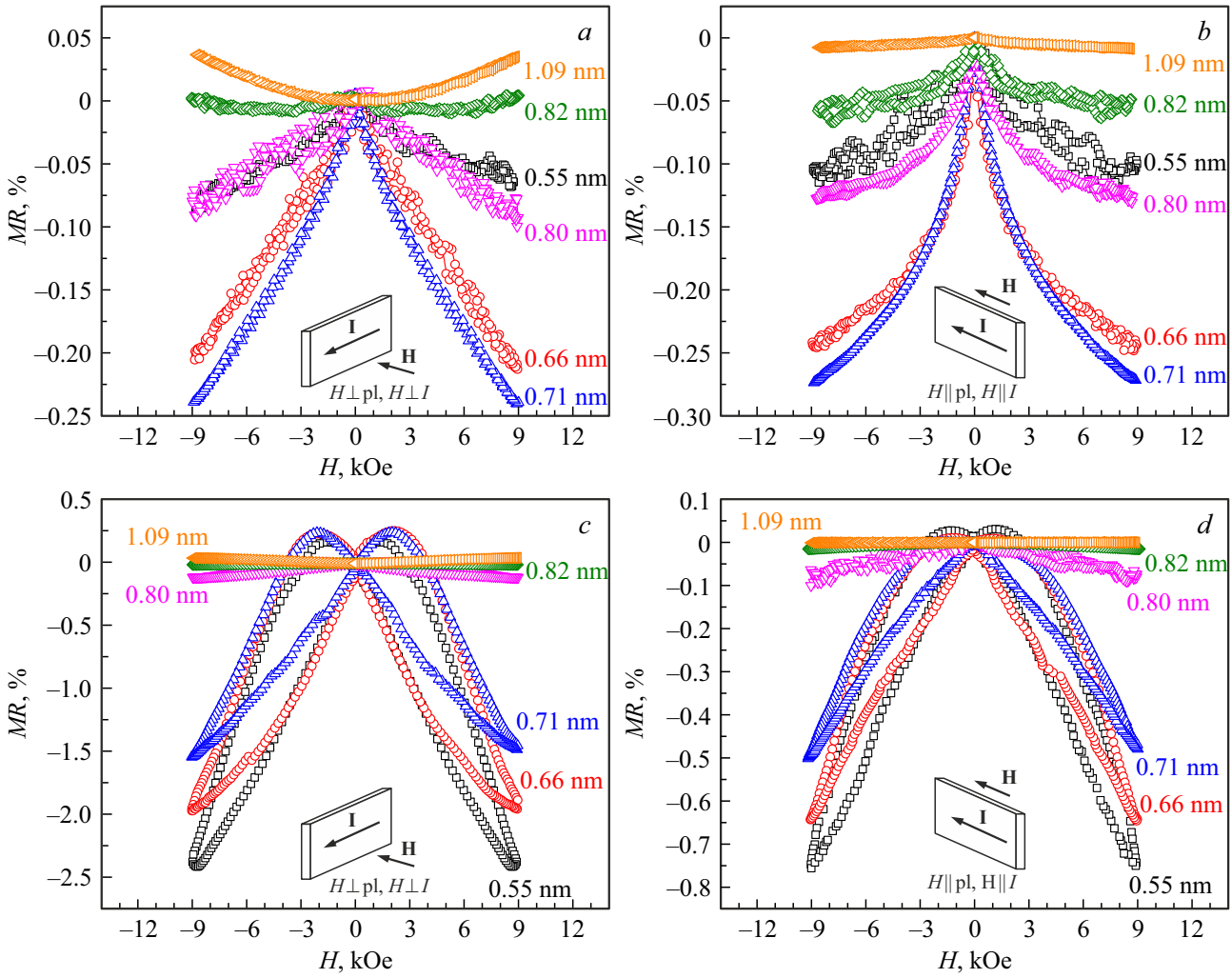

Figure 12. Dependences of the magnetoresistance MR on the strength of an external magnetic field H for multilayer thin films $(Co/CoO)_{60}$, measured at a temperature of 300 K: ($H \perp$ pl, $H \perp I$) (*a*), ($H \parallel$ pl, $H \parallel I$) (*b*); measured at a temperature of 77 K: ($H \perp$ pl, $H \perp I$) (*c*), ($H \parallel$ pl, $H \parallel I$) (*d*). The figures for the curves show the values of the thickness of the layers Co.

In the case when the magnetic field is directed in the plane of the film, and the electric current is directed parallel to HA, the field dependences of MR practically coincide (curves *1* and *2* Figure 13, *a*). The magnetic moments of conducting percolation Co clusters in the absence of an external magnetic field are oriented mainly along the EA (perpendicular to the HA), forming a cone. At $H \parallel$ pl, $H \parallel I$, $I \parallel$ EA in the absence of an external field, the magnetic moments are oriented along the axis of the cone of the EA, and the application of an external field will lead to their orientation along the current direction, which, according to the AMR model in ferromagnets should lead to an increase in resistance (to positive MR), however, as can be seen from Figure 13, *a* (curve *1*) this does not correspond to the experimental results. A similar contradiction is observed under the conditions when $H \parallel$ pl, $H \parallel I$, $I \parallel$ HA (curve *4* Figure 13, *a*), for which the application of an external magnetic field leads to a decrease in the angle of solution of the cone formed by magnetic moments, thus reducing the component perpendicular to the current, which should also lead to a positive MR. This is atypical for the AMR observed in ferromagnetic materials, in particular Co [22], which can be explained both by the presence of components of EA and HA perpendicular to the plane of the film, and by the presence of additional mechanisms of negative MR, discussed earlier in the work [25] for multilayer systems $(ZnO/C)_{25}$.

On the other hand, for the cases when $H \parallel$ pl, $H \perp I$ the external field orients the magnetic moments perpendicular to the direction of current propagation (curves *2* and *5* Figure 13, *a*), which leads to the appearance of a negative MR, while the change in resistance is maximum for the case when $I \parallel$ HA (curve *5* Figure 13, *a*). This is consistent with the AMR model of ferromagnetic materials, since when an external field is applied in the case of $H \parallel$ pl, $H \perp I$, $I \parallel$ EA (curve *2* Figure 13, *a*), the angle of the cone solution formed by magnetic moments decreases, thus reducing the longitudinal current component.

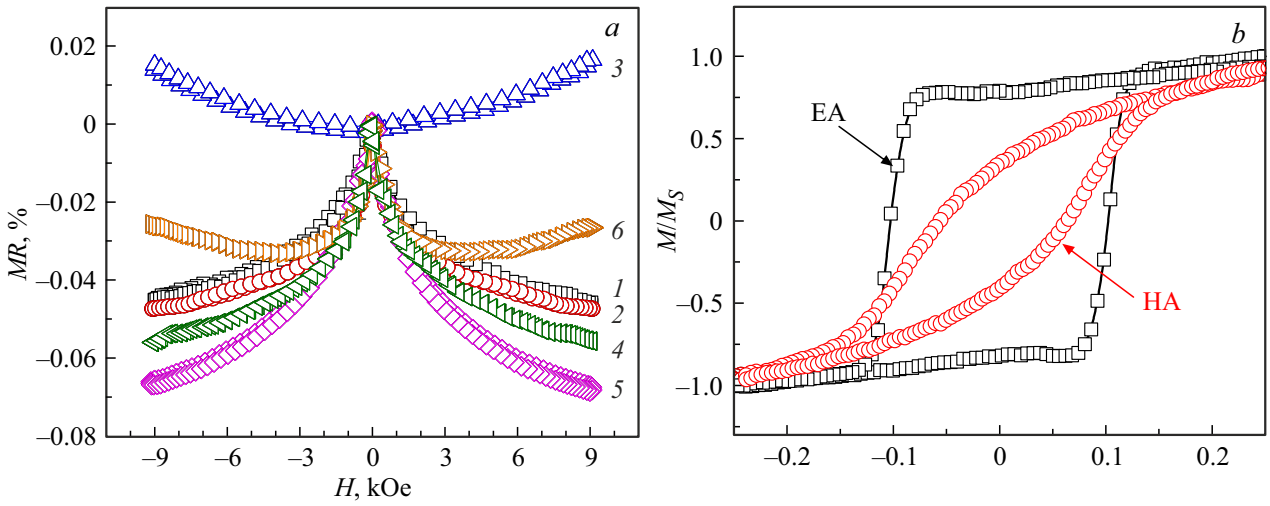

Figure 13. Field dependences of magnetoresistance (*a*): (*1* — $H \parallel$ pl, $H \parallel I$, $I \parallel$ EA; *2* — $H \parallel$ pl, $H \perp I$, $I \parallel$ EA; *3* — $H \perp$ pl, $H \perp I$, $I \parallel$ EA; *4* — $H \parallel$ pl, $H \parallel I$, $I \parallel$ HA; *5* — $H \parallel$ pl, $H \perp I$, $I \parallel$ HA; *6* — $H \perp$ pl, $H \perp I$, $I \parallel$ HA) and hysteresis loops MOKE (*b*) (EA is the magnetic field is directed along the easy axis, HA is the magnetic field directed along the hard axis), measured at room temperature for a multilayer thin film $(Co/CoO)_{60}$ with an equivalent interlayer thickness of 0.84 nm (near the percolation threshold).

For the case when the magnetic field was directed perpendicular to the film plane ($H \perp$ pl), and therefore to the current direction ($H \perp I$) (curves *3* and *6* Figure 13, *a*), the MR contained two contributions (positive and negative) when the electric current was directed along the EA (curve *6* Figure 13, *a*) and was only positive when the electric current was directed along the HA (curve *3* Figure 13, *a*).

Under such measurement conditions, the external magnetic field tends to orient the magnetic moments of percolation Co clusters perpendicular to the film plane and the direction of the electric current, which, provided that the AMR is implemented, would lead to a decrease in resistance and, consequently, to a negative MR. Valid for the sample with $I \parallel$ HA provided $H \perp$ pl, $H \perp I$ (curve *6* Figure 13, *a*) in the area of weak fields (no more than 3 kOe) there is a negative component. A further increase in the strength of the external field for this sample leads to a positive contribution to MR.

The magnetic moments of percolation Co clusters are located predominantly perpendicular to the direction of electric current flow in the film plane for a sample with $I \parallel$ EA ($I \perp$ HA) in the absence of an external field. The magnetic moments will be oriented perpendicular to the film plane with an increase in the external field and the conditions $H \perp$ pl, $H \perp I$, but the mutual orientation of the sample magnetization and current will not change. For this reason no negative contribution of MR is observed for a sample with $H \perp$ pl, $H \perp I$, $I \parallel$ EA, and an increase in the magnetic field leads to an increase in MR (curve *3* Figure 13, *a*).

It should be noted that the dependence of the positive MR is close to parabolic at room temperature (curves *3* and *6* Figure 13, *a*), no magnetic hysteresis is observed. Such dependences may be a consequence of the presence of classical Lorentz magnetoresistance, which is a consequence of the curvature of the trajectory of charge carriers (electrons) in a magnetic field.

Thus, the magnetoresistance of thin films $(Co/CoO)_{60}$ up to the percolation threshold is determined by the mechanism of spin-dependent tunneling between granules and clusters of metallic Co, and beyond the threshold by competing contributions from the anisotropic magnetoresistance of the ferromagnetic cobalt percolation grid and Lorentz magnetoresistance.

4. Conclusion

Thin films $(Co/CoO)_{60}$ were obtained by ion beam sputtering of a ceramic target of Co and metallic Co and subsequent layer-by-layer deposition in an argon atmosphere. A study of the structure by XRD and TEM methods has shown that the obtained films are multilayer, while an increase in the equivalent thickness of the Co interlayer to 0.8 nm leads to a transition from island layers of Co in a continuous CoO matrix to a multilayer structure consisting of continuous layers of metallic Co and non-conductive electric current CoO.

The temperature dependences of the specific electrical conductivity of thin films $(Co/CoO)_{60}$ have been experimentally studied. It was found that at values of the equivalent thickness of the Co interlayer up to 0.8 nm (up to the percolation threshold) in the temperature range 80–280 K, the dominant transfer mechanism from the hopping conduction mechanism to localized states near the Fermi level with a variable hopping length (80–140 K) to nearest adjacent hops (140–280 K). For thin films $(Co/CoO)_{60}$ located beyond the percolation threshold, the conductivity

is determined by two-dimensional grids of metal granules and is characterized by a positive temperature coefficient.

The magnetic properties of a multilayer film $(Co/CoO)_{60}$ were studied using methods based on measuring the magneto-optical Kerr effect and using a vibrating magnetometer. The study results showed the presence of magnetic anisotropy in the samples near and beyond the percolation threshold, while the axes of light and hard magnetization are in the plane of the film and perpendicular to each other.

A study of the dependences of the electrical resistance of thin films $(Co/CoO)_{60}$ on the magnetic field strength showed that the magnetoresistance is determined by the mechanism of spin-dependent tunneling between granules and clusters of metallic Co for samples up to the percolation threshold, and beyond the threshold by competing contributions from the anisotropic magnetoresistance of the ferromagnetic cobalt percolation grid and Lorentz magnetoresistance.

Funding

The study was supported by the Ministry of Science and Higher Education of the Russian Federation within the framework of the state order (project No. FZGM-2023-0006).

Conflict of interest

The authors declare no conflict of interest.

References

[1] [K.Y. Constantinian, G.A. Ovsyannikov, A.V. Shadrin, V.A. Shmakov, A.M. Petrzhik, Yu.V. Kislinskii, A.A. Klimov. Phys. Solid State **64**, *10*, 1410 (2022). DOI: 10.21883/PSS.2022.10.54227.46HH
[2] A.V. Svalov, G.V. Kurlyandskaya, V.O. Vas'kovskiy, A. Larranaga, R. Domingues Della Pace, C.C. Plś Cid. Journal of Non–Crystalline Solids. **90**, 242 (2016). DOI: 10.1016/j.spmi.2015.12.030
[3] I.G. Vazhenina, S.V. Stolyar, V.Y. Yakovchuk, M.V. Rautsky, R.S. Iskhakov. JETP Lett. **48**, *5*, 38 (2022). DOI: 10.21883/TPL.2022.05.53477.19135
[4] A.V. Sitnikov, V.A. Makagonov, Y.E. Kalinin, S.B. Kushchev, V.A. Foshin, N.N. Perova, E.A. Ganshina, A.B. Granovsky. JMMM **587**, 171154 (2023). DOI: 10.1016/j.jmmm.2023.171154.
[5] A.B. Rinkevich, M.A. Milyaev, E.A. Kuznetsov, D.V. Perov, A.Y. Pavlova. JETP **67**, *4*, 515 (2022). DOI: 10.21883/TP.2022.04.53609.298-21
[6] S. Yoshida, H. Ono, S. Ando, F. Tsuda, T. Ito, Y. Shimada, M. Yamaguchi, K. Arai, S. Ohnuma T. Masumoto. IEEE **37**, *4*, 2401 (2011). DOI: 10.1109/20.951185
[7] P.M. Raj, P. Muthana, T.D. Xiao, L. Wan, D. Balaraman, I.R. Abothu, S. Bhattacharya, M. Swaminathan, R. Tummala. IEEE **272** (2005). DOI: 10.1109/ISAPM.2005.1432088
[8] R.G. Mitarov, S.N. Kallaev, Z.M. Omarov, K.G. Abdulvakhidov. Phys. Solid State **65**, *2*, 355 (2023). DOI: 10.21883/PSS.2023.02.55423.526
[9] V.V. Koledov, E.T. Dilmieva, V.S. Kalashnikov, A.P. Kamantsev, A.V. Mashirov, S.V. Von Gratovsky, V.G. Shavrov, Yu.S. Koshkidko, A.V. Koshelev, S.V. Taskaev, V. Sampat, I.I. Musabirov, F.V. Chung, R.M. Grechishkin. Journal of radio electronics **7** (2018). DOI: 10.30898/1684-1719.2018.7.8
[10] V.S. Kalashnikov, V.V. Koledov, V.G. Shavrov, V.A. Andreev, A.V. Nesolenov, D.S. Kuchin, R.D. Karelin. Radiotekhnika i elektronika (in Russian) **68**, *4*, 338 (2023). DOI: 10.31857/S0033849423040046
[11] V.V. Rylkov, S.N. Nikolaev, V.A. Demin, A.V. Yemelyanov, A.V. Sitnikov, K.E. Nikitui, V.A. Levanov, M.Y. Presnyakov, A.N. Taldenkov, A.L. Vasiliev, K.Y. Chernoglazov, A.S. Vedeneev, Yu.E. Kalinin, A.B. Granovsky, V.V. Tugushev, A.S. Bugaev. JETP **126**, *3*, 353 (2018). DOI: 10.1134/S1063776118020152
[12] A.B. Drovosekov, N.M. Kreines, A.S. Barkalova, S.N. Nikolaev, V.V. Rylkov, A.V. Sitnikov. JMMM **495**, 165875 (2020). DOI: 10.1016/j.jmmm.2019.165875
[13] L.N. Kotov, V.S. Vlasov, V.A. Ustyugov, V.K. Turkov, M.Yu. Dianov, Yu.E. Kalinin, A.V. Sitnikov, E.A. Golubev. IOP Conf. Ser.: Mater. Sci. Eng. **175**, 012021 (2017). DOI: 10.1088/1757-899X/175/1/012021
[14] J. van Lierop, K.-W. Lin, J.-Y. Guo, H. Ouyang, B.W. Southern. Phys. Rev. B **75**, *13*, 134409 (2007). DOI: 10.1103/PhysRevB.75.134409
[15] K. Lenz, S. Zander, W. Kuch. Phys. Rev. Lett. **98**, 237201 (2007). DOI: 10.1103/PhysRevLett.98.237201
[16] S.A. Gridnev, Yu.E. Kalinin, A.V. Sitnikov, O.V. Stogney. Nelinejnye yavleniya v nano- i mikrogeterogennykh sistemakh. BINOM. Laboratoriya znanij, M. (2012). p. 352. (in Russian).
[17] F.J. Blatt, P.A. Schroeder, K.L. Foyles, D. Greig. Thermoelectromotive force of metals: translated from English. I.A.Magidson; edited by D.K.Belashchenko. Metallurgiya, M. (1980). p. 247. (in Russian).
[18] N.F. Mott, E.A. Davies. Electron Processes in Non-Crystalline Materials (Clarendon, Oxford, 1979).
[19] O.V. Stogney, A.A. Grebennikov. Vestnik Voronezhskogo gosudarstvennogo universiteta **6**, *1*, 173 (2010). (in Russian).
[20] O.V. Stogneĭ, A.V. Sitnikov, Y.E. Kalinin, S.F. Avdeev, M.N. Kopytin. Phys. Solid State **49**, *1*, 164 (2007). DOI: 10.1134/S106378340701026X
[21] S.V. Vonsovsky Magnetizm. Nauka, M. (1971). p. 1032. (in Russian).
[22] M. El-Tahawy, L. Péter, L.F. Kiss, J. Gubicza, Zs. Czigány, G. Molnár, I. Bakonyi. JMMM **560**, 169660 (2022). DOI: 10.1016/j.jmmm.2022.169660
[23] N.S. Akulov Ferromagnetizm. OGIZ, M. (1939). p. 188. (in Russian).
[24] P. Ritzinger, K. Výborný. R. Soc. Open Sci. **10**, 230564 (2023). DOI: 10.1098/rsos.230564
[25] E.A. Fadeev, E. Lahderanta, B.A. Aronzon, A.B. Mekhiya, Yu.E. Kalinin, V.A. Makagonov, S.Yu. Pankov, V.A. Foshin, A.B. Granovsky. JMMM **535**, 167963 (2021). DOI: 10.1016/j.jmmm.2021.167963

Translated by A.Akhtyamov